ACS APPLIED MATERIALS & INTERFACES

Research Article

www.acsami.org

High-Crystalline Medium-Band-Gap Polymers Consisting of Benzodithiophene and Benzotriazole Derivatives for Organic Photovoltaic Cells

Ji-Hoon Kim,[†] Chang Eun Song,[‡] Nara Shin,[⊥] Hyunbum Kang,[▽] Sebastian Wood,[¶] In-Nam Kang,[§] Bumjoon J. Kim,[▽] BongSoo Kim,[⊥] Ji-Seon Kim,[¶] Won Suk Shin,[∥] and Do-Hoon Hwang*[,†]

[†]Department of Chemistry and Chemistry Institute for Functional Materials, Pusan National University, Busan 609-735, Republic of Korea

[‡]Department of Materials Science and Engineering, Korea Advanced Institute of Science and Technology, Daejeon 305-701, Republic of Korea

[§]Department of Chemistry, The Catholic University of Korea, Bucheon 420-743, Republic of Korea

[⊥]Photo-electronic Hybrids Research Center, Korea Institute of Science and Technology (KIST), Seoul 136-791, Republic of Korea

[∥]Korea Research Institute of Chemical Technology, 100 Jang-dong, Yuseong-gu, Daejeon 305-343, Republic of Korea

[¶]Department of Physics and Centre for Plastic Electronics, Imperial College London, London SW7 2AZ, United Kingdom

[▽]Department of Chemical and Biomolecular Engineering, Korea Advanced Institute of Science and Technology, Daejeon 305-701, Republic of Korea

Supporting Information

ABSTRACT: Two semiconducting conjugated polymers were synthesized via Stille polymerization. The structures combined unsubstituted or (triisopropylsilyl)ethynyl (TIPS)-substituted 2,6-bis(trimethylstannyl)benzo[1,2-*b*:4,5-*b*′]dithiophene (BDT) as a donor unit and benzotriazole with a symmetrically branched alkyl side chain (DTBTz) as an acceptor unit. We investigated the effects of the different BDT moieties on the optical, electrochemical, and photovoltaic properties of the polymers and the film crystallinities and carrier mobilities. The optical-band-gap energies were measured to be 1.97 and 1.95 eV for PBDT-DTBTz and PTIPSBDT-DTBTz, respectively. Bulk heterojunction photovoltaic devices were fabricated and power conversion efficiencies of 5.5% and 2.9% were found for the PTIPSBDT-DTBTz- and PBDT-DTBTz-based devices, respectively. This difference was explained by the more optimal morphology and higher carrier mobility in the PTIPSBDT-DTBTz-based devices. This work demonstrates that, under the appropriate processing conditions, TIPS groups can change the molecular ordering and lower the highest occupied molecular orbital level, providing the potential for improved solar cell performance.

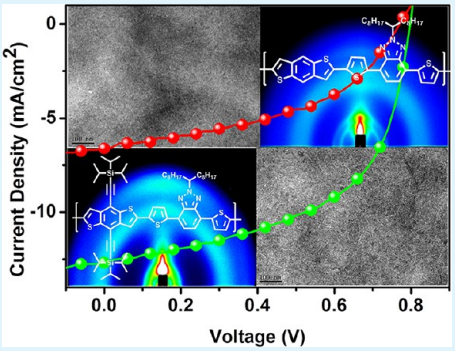

KEYWORDS: *organic photovoltaic device, medium-band-gap polymer, (triisopropylsilyl)ethynyl-substituted benzodithiophene, 2D-GIXS, resonant Raman spectroscopy*

INTRODUCTION

In recent years, bulk-heterojunction (BHJ) photovoltaic cells have become one of the most promising solutions to our increasing need for alternatives to oil-based energy sources. Their ability to be manufactured at low cost, in addition to their flexibility and lightweight properties, affords them great potential in the field of renewable energy generation.[1−5] By developing novel polymers and device structures and improving processing methods for high-performance BHJ photovoltaic cells, researchers have achieved power conversion efficiencies (PCEs) exceeding 9.0% from single organic photovoltaic (OPV) cells.[6−10] Most recent research has focused on the design and synthesis of low-band-gap (typically, E_g < 1.7 eV) donor polymers[11] in order to enable utilization of a wider region of the solar spectrum. At the same time, it has been essential to keep the highest occupied molecular orbital (HOMO) level of the polymers deep and the lowest unoccupied molecular orbital (LUMO) of the acceptors high, allowing large open-circuit voltages (V_{oc}) and efficient exciton separation, respectively, to be achieved. However, medium-band-gap polymers (E_g = 1.7−2.0 eV) have been generally overlooked despite them being an important class of OPV materials that are able to produce a higher V_{oc} than low-band-gap polymers owing to their deep HOMO energy levels.[12−15]

Received: May 21, 2013
Accepted: August 1, 2013
Published: August 1, 2013

Scheme 1. Synthetic Routes and Chemical Structures of DTBTz Monomers

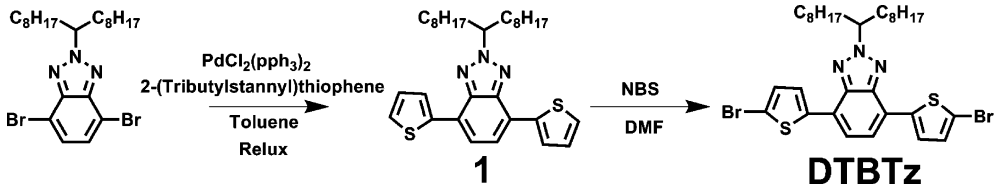

Scheme 2. Synthetic Routes and Chemical Structures of Electron-Donating Monomers

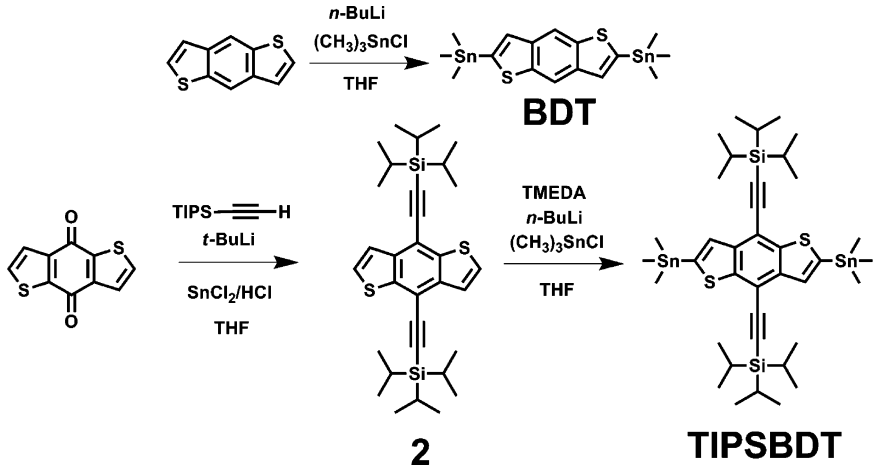

In particular, they can play a significant role in the development of OPV tandem cells that consist of two (or more) stacked cells. Each photoactive layer in each stacked cell absorbs a specific range of the solar spectrum.[10]

Blouin et al. reported the synthesis of one of most representative medium-band-gap polymers, poly[*N*-9′-heptadecanyl-2,7-carbazole-*alt*-5,5-(4′,7′-di-2-thienyl-2′,1′,3′-benzothiadiazole)] (PCDTBT; $E_g \approx 1.9$ eV).[16] The photovoltaic devices fabricated using PCDTBT exhibited the maximum PCE of 3.6%. The PCE of the PCDTBT device was much improved up to 6.9% by further optimization of the devices.[17] Price et al. also reported the synthesis of a medium-band-gap polymer, poly[4,8-(3-hexylundecyl)benzo[1,2-*b*:4,5-*b*′]dithiophene-*alt*-4,7-bis(thiophen-2-yl)-2-(2-butyloctyl)-5,6-difluoro-2*H*-benzo[*d*][1,2,3]triazole] (PBnDT-FTAZ), which showed the maximum PCE of 7.1%.[18] For the bottom cell component of the tandem OPVs, poly(3-hexylthiophene) (P3HT) has been the state of the art of medium-band-gap polymers because of its reliable and high photovoltaic performances.[10] Its PCE has been shown to be typically in the range of 3.0−4.0% when blended with [6,6]-phenyl C_{61}-butyric acid methyl ester ($PC_{61}BM$) and was further improved up to 5.0% by various processing optimizations and device modifications.[3,19] However, its absorption in the long-wavelength range usually overlaps with the short-wavelength absorption region of low-band-gap polymer cells. This spectral overlapping is a disadvantage for tandem solar cell PCEs. Thus, the development of new highly efficient medium-band-gap polymers with the absorption blue-shifted to some degree compared to P3HT is emerging as a promising method by which to improve the PCEs of tandem solar cells.[10] Unfortunately, the reported efficiencies of medium-band-gap polymers are still low, being typically ∼3.0%,[20] with the exception of a recently reported value of 5.04%.[21] Therefore, new medium-band-gap polymers with high PCEs and a simple device fabrication process are desirable.

In this study, we prepared novel medium-band-gap copolymers consisting of benzotriazole (BTz) moieties substituted with symmetrically branched alkyl side chains as an electron-accepting part and aromatic fused systems substituted with (triisopropylsilyl)ethynyl (TIPS) groups as an electron-donating part. Recently, we reported an effective method for enhancing the interchain interaction between conjugated polymer chains, whereby a symmetrically branched alkyl side chain was introduced on the center nitrogen atom in the BTz unit. This D−A-type polymer exhibited a deeper HOMO level and higher hole mobility than those with the same backbone but with linear alkyl side chains.[22] To utilize these benefits and ensure polymer solubility, in the present study, we introduced the same symmetrically branched alkyl side chains to the electron-accepting BTz unit.

It is well-known that bulky TIPS groups on acene derivatives not only improve the solubility, crystallinity, and oxidative stability of the semiconductors but also promote π-orbital overlap between conjugated molecules.[23,24] TIPS-functionalized acenes have thus gained importance in the design of highly soluble, air-stable, high-performance p-type organic semiconductors. TIPS-substituted small molecules have been used as electron donors in OPV cells, with the highest reported PCE values being up to 2.25%.[25,26] Li and co-workers reported that the conjugated polymer PBDTTT-TIPS containing benzodithiophene (BDT) substituted with TIPS groups gave a high V_{oc} of 0.89 V and a PCE of 4.33%. This work demonstrated the potential of TIPS groups in comparison to linear alkyl chains for use in OPVs.[27,28]

In this study, we synthesized two new medium-band-gap copolymers, PBDT-DTBTz and PTIPSBDT-DTBTz, by combining unsubstituted BDT or TIPS-substituted BDT (TIPSBDT) as a donor unit and BTz with a symmetrically

Scheme 3. Synthetic Routes and Chemical Structures of PBDT-DTBTz and PTIPSBDT-DTBTz

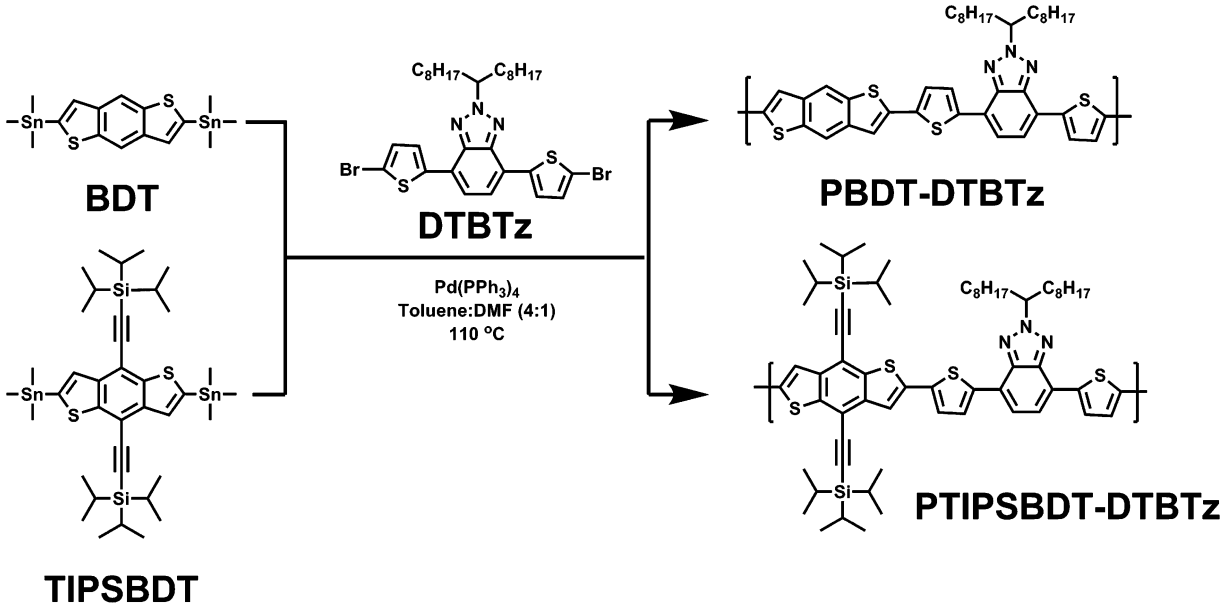

branched alkyl side chain [4,7-bis(5-bromothiophen-2-yl)-2-(heptadecan-9-yl)-2*H*-benzo[*d*][1,2,3]triazole (DTBTz)] as an acceptor unit. The optical, electrochemical, and photovoltaic properties were investigated, in addition to the mobility and crystallinity. It was found that although the TIPS groups did not change the optical gaps, they lowered the HOMO level effectively and enhanced hole transport via increased crystallinity. BHJ photovoltaic devices constructed using PTIPSBDT-DTBTz/$PC_{71}BM$ blends gave a high PCE of 5.5%, while PBDT-DTBTz/$PC_{71}BM$-based devices exhibited a moderate PCE of 2.9%. The photovoltaic difference could be attributed to the more optimal morphology and higher carrier mobility in the PTIPSBDT-DTBTz/$PC_{71}BM$-based devices. Overall, this work demonstrates that the TIPS group is a potentially important polymer backbone substituent for the development of high-performance solar cells.

RESULTS AND DISCUSSION

Polymer Synthesis and Characterization. The monomers were synthesized according to methods previously reported in the literature (Schemes 1 and 2).[29] The two polymers, PBDT-DTBTz and PTIPSBDT-DTBTz, were synthesized using Stille cross-coupling polymerization in the presence of a $Pd(PPh_3)_4$ catalyst (Scheme 3).[29] All of the polymers were found to have good solubility in common organic solvents such as chloroform, chlorobenzene, and toluene and were able to be formed into uniform thin films using spin coating. The number-average molecular weights (M_n) and polydispersity indices (PDIs) of the polymers were determined using gel permeation chromatography (GPC) analysis with a polystyrene standard calibration. The M_n values for PBDT-DTBTz and PTIPSBDT-DTBTz were found to be 15000 and 23000 g mol^{-1}, with corresponding PDIs of 2.6 and 2.5, respectively (Table 1).

The thermal stability of the polymers was investigated using thermogravimetric analysis (TGA), which revealed that the 5% weight loss (T_d) temperatures of PBDT-DTBTz and PTIPSBDT-DTBTz were 425 and 413 °C, respectively (Figure S1 in the Supporting Information). This indicates that the thermal stability of both polymers was sufficient for application to optoelectronic devices.

Table 1. Average Molecular Weights and Thermal Properties of the Synthesized Polymers

polymer	polymer yield (%)	M_n[a] (g mol^{-1})	M_w[a] (g mol^{-1})	PDI[a]	T_d[b] (°C)
PBDT-DTBTz	55	15000	40000	2.1	425
PTIPSBDT-DTBTz	54	23000	57000	2.5	413

[a]M_n, M_w, and PDIs of the polymers were determined by GPC using polystyrene standards in $CHCl_3$. [b]Temperature at 5% weight loss with a heating rate of 10 °C min^{-1} under nitrogen.

Optical Properties. Parts a and b of Figure 1 show the UV−visible absorption spectra measured for PBDT-DTBTz and PTIPSBDT-DTBTz in a chloroform solution and in the film state, respectively. The two solution spectra can be seen to have similar profiles with two major peaks owing to $\pi-\pi^*$ transitions of the conjugated polymer backbones. However, the absorption band and peak maximum for PTIPSBDT-DTBTz are red-shifted by approximately 20 nm compared with those of PBDT-DTBTz, even though the absorption edges of the two polymers are similar. This red shift was attributed to extension of the effective π-conjugation length by the acetylene units in TIPS groups in PTIPSBDT-DTBTz.

The spectra from the polymer thin films had a trend to similar that found for the solutions (Figure 1b); however, the absorption bands were shifted toward the longer-wavelength region because of the stronger interactions between the polymer chains in the solid state. Interestingly, the shoulder absorption peaks in the longer-wavelength region became stronger and sharper than those in the corresponding polymer solutions, indicating that a highly ordered structure is present in the polymer films.[30] Compared to the absorption spectrum of a P3HT film (E_g ~1.9 eV; Figure 1b), the shapes of the absorption bands from the polymer films synthesized in the present study are quite similar, but as intended, they are slightly blue-shifted. The optical band gaps (E_g^{opt}) of the polymer thin films were determined from their UV−visible absorption edges

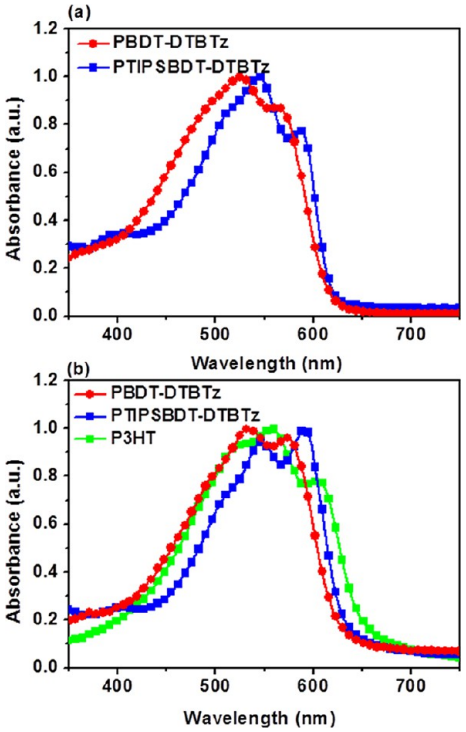

Figure 1. Normalized UV−visible absorption spectra of (a) polymers in a chloroform solution and (b) in thin films.

to be 627 nm (1.97 eV) for PBDT-DTBTz and 635 nm (1.95 eV) for PTIPSBDT-DTBTz.

Theoretical Calculations. To obtain information on the HOMO/LUMO energy levels and electronic density distributions of the polymers, molecular calculation was conducted. For the calculations, we designed two D−A−D−A structured model compounds, $(BDT\text{-}DTBTz)_2$ and $(TIPSBDT\text{-}DTBTz)_2$. The model compounds were analyzed using density functional theory (DFT) with *DMol3* software.[22,31,32] Parts a and b of Figure 2 show the structures of the model compounds and their simulated front-view structures, and Figure 2c shows the HOMO/LUMO energy levels and the electron distributions of model compounds.

Several important observations were made. First, the conformation of the molecular backbone was quite flat and almost independent of the substitution with the TIPS groups. Second, the electronic density in the HOMO of $(BDT\text{-}DTBTz)_2$ was well distributed along the conjugated main chain, while that in the LUMO was localized near the electron-accepting DTBTz unit, that is, between the electron-donating BDT units. The electron density distribution in the HOMO of $(TIPSBDT\text{-}DTBTz)_2$ was similar to that in the HOMO of $(BDT\text{-}DTBTz)_2$. However, the electron density in the LUMO of $(TIPSBDT\text{-}DTBTz)_2$ was better spread out along the main chain than that in the LUMO of $(BDT\text{-}DTBTz)_2$ because of the relatively electronegative sp-hybridized carbon atoms in the TIPS unit. As a result, the band-gap energy of the $(TIPSBDT\text{-}DTBTz)_2$ model compound was slightly smaller than that of $(BDT\text{-}DTBTz)_2$. This characteristic is consistent with the values of E_g^{opt} measured for the polymers. Lastly, the HOMO/LUMO energy levels of $(TIPSBDT\text{-}DTBTz)_2$ were slightly deeper than those corresponding to $(BDT\text{-}DTBTz)_2$ because of the contribution of the electronegative sp-hybridized carbon atoms in the TIPS groups.

Electrochemical Properties. The HOMO energy levels were determined from the oxidation onsets (E_{ox}) of the polymer films by cyclic voltammetry (CV).[27,33] The obtained CV curves of the polymers are shown in Figure S2 in the Supporting Information. In the anodic scan, the onsets of oxidation for PBDT-DTBTz and PTIPSBDT-DTBTz occurred at 0.55 and 0.69 V, corresponding to ionization potential values of −5.26 and −5.40 eV, respectively. The lower HOMO level observed for PTIPSBDT-DTBTz could be attributed to the electron-withdrawing TIPS units, as described above. In general, the large difference between the HOMO level of a donor polymer and the LUMO level of an acceptor increases the V_{oc} values of OPVs.[11] In this regard, higher V_{oc} values can be expected for the polymers synthesized in this study compared to those found for P3HT-based devices (∼0.6 V) because both polymers displayed lower HOMO levels than those of P3HT (−4.6 to −5.1 eV).[34,35]

The LUMO levels of the polymers were determined from the HOMO levels obtained from the CV measurements and the E_g^{opt} values obtained from the UV−visible absorption edges. The LUMO levels of PBDT-DTBTz and PTIPSBDT-DTBTz were estimated to be −3.29 and −3.45 eV, respectively, providing a large enough offset between their LUMO levels and that of $PC_{71}BM$ to ensure efficient exciton separation.[24,36] It should be noted that the basic HOMO/LUMO trend is consistent with that predicted using the theoretical calculations, demonstrating the utility of the model compounds for explaining the experimental data. Accordingly, the HOMO and LUMO energy levels of the polymers are illustrated in Figure 2d. The optical and electrochemical properties of the polymers are summarized in Table 2.

Two-Dimensional Grazing Incidence X-ray Scattering (2D-GIXS) and Structural Properties. 2D-GIXS measurements were conducted to probe the crystallinity and crystal orientation of the polymer films. The samples were prepared by spin-coating polymer solutions onto PEDOT:PSS (40−50 nm)-coated silicon wafers.[37] Parts a and b of Figure 3 show the 2D-GIXS images of the PBDT-DTBTz and PTIPSBDT-DTBTz films, respectively. Figure 3a shows a more resolved lamellar peak at q_y = 0.36 Å^{-1} (d = 17.5 Å) in the in-plane direction than in the out-of-plane direction. In addition, a weak peak is evident at q_z = ∼1.73 Å^{-1} (d = 3.63 Å) in the out-of-plane direction, corresponding to π−π stacking between polymer chains. These two observations suggest that PBDT-DTBTz is weakly crystalline with a mainly face-on orientation with respect to the substrate. In contrast, Figure 3b shows that, while PTIPSBDT-DTBTz exhibited similar features, the crystalline peaks are more pronounced. That is, both the lamellar peak at q_y = 0.25 Å^{-1} (d = 25.1 Å) in the in-plane direction and the π−π-stacking peak at q_z = ∼1.72 Å^{-1} (d = 3.65 Å) in the out-of-plane direction are clearer. This observation indicates that the bulky TIPS groups induce a more crystalline lamellar structure by promoting polymer interchain stacking. This has several important implications: (i) the face-on orientation of the polymer films is desirable for photovoltaic devices, where holes move in the vertical direction toward the anodic electrode, (ii) the small π−π-stacking distance of ∼3.65 Å compared to typical semiconducting polymers would facilitate hole transport, and (iii) the increased crystallinity of PTIPSBDT-DTBTz compared to PBDT-DTBTz explains its 5 times higher hole mobility (see below).

Organic Thin-Film Transistor (OTFT) Characteristics. The field-effect carrier mobilities of the polymers were

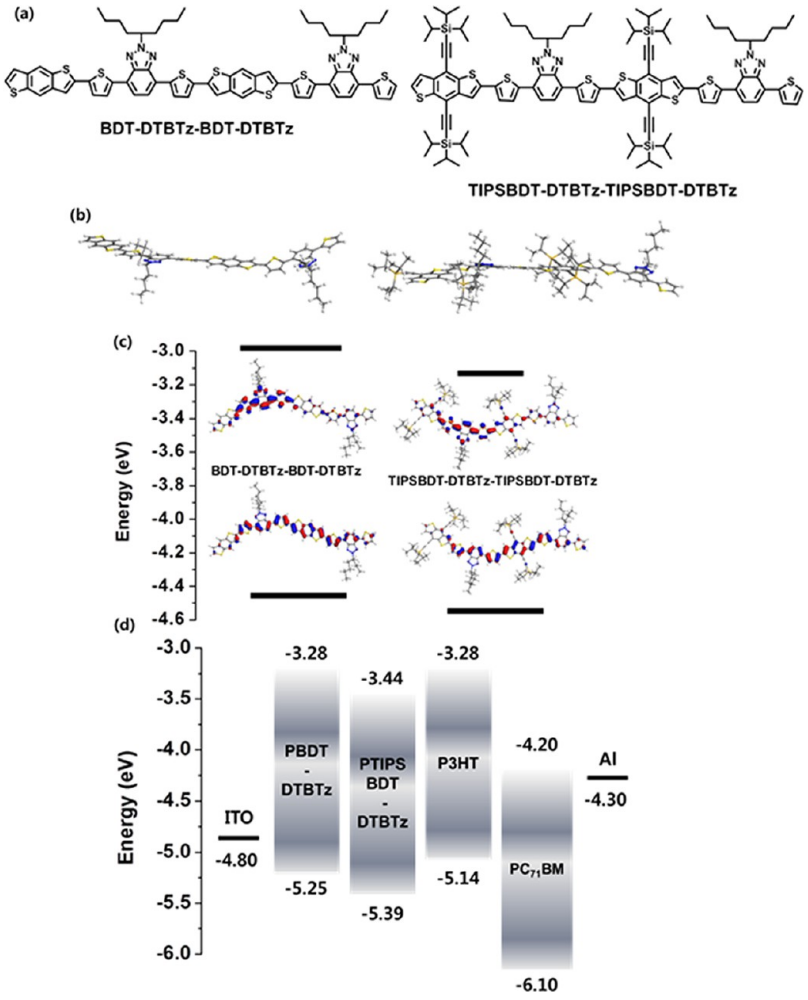

Figure 2. (a) Chemical structures of the model compounds, (b) calculated molecular structures (front views), (c) calculated energy levels and the electronic distributions of the HOMO/LUMO frontier orbitals of the model compounds, and (d) energy level diagram of the synthesized polymers P3HT, $PC_{71}BM$, ITO, and aluminum electrodes.

Table 2. Optical and Electrochemical Properties of the Synthesized Polymers

	solution[a]	film[b]					
polymer	$\lambda_{max,abs}$ (nm)	λ_{max} (nm)	λ_{edge} (nm)	optical E_g^{opt} (eV)[c]	E_{onset}^{ox}	HOMO (eV)[d]	LUMO (eV)[e]
PBDT-DTBTz	526	535, 573	627	1.97	−0.55	−5.26	−3.29
PTIPSBDT-DTBTz	544	548, 592	635	1.95	−0.69	−5.40	−3.45

[a] 1×10^{-5} M in anhydrous chloroform. [b] Polymer film on a quartz plate by spin coating from a solution in chloroform at 1500 rpm for 30 s. [c] Calculated from the UV−visible absorption edge of the polymer films, $E_g = 1240/\lambda_{edge}$. [d] HOMO = −e($E_{onset}^{ox}$ + 4.70) (eV). [e] LUMO = E_g^{opt} + HOMO (eV).

measured using a TFT test bed with a bottom-contact geometry using an OTS-treated SiO_2 dielectric and gold source/drain electrodes. Figure 4 shows the transfer curves for the TFTs of the polymers, where it can be seen that they exhibited typical p-channel TFT characteristics. The TFT mobilities were calculated in the saturation region using the following equation:

$$I_{ds} = (WC_i/2L)\mu(V_G - V_T)^2$$

where I_{ds} is the drain/source current in the saturated region, W and L are the channel width (120 μm) and length (12 μm), respectively, μ is the field-effect mobility, C_i is the capacitance per unit area of the insulation layer (SiO_2, 300 nm), and V_G and V_T are the gate and threshold voltages, respectively.[38,39] The OTFTs fabricated using PBDT-DTBTz and PTIPSBDT-DTBTz showed hole mobilities of 7.4×10^{-4} and 3.8×10^{-3} $cm^2\ V^{-1}\ s^{-1}$, respectively. It should be noted that these are comparable to, or exceed, the value of 10^{-3} $cm^2\ V^{-1}\ s^{-1}$ that has been proposed to be necessary in order to reduce the photocurrent loss and obtain high-performance OPV devices.[40] The higher mobility of PTIPSBDT-DTBTz is attributed to its higher crystallinity compared to PBDT-DTBTz, as revealed by 2D-GIXS analysis.

Resonant Raman Spectroscopy. Figure 5a shows the Raman spectra measured for thin films of PBDT-DTBTz and PTIPSBDT-DTBTz using a 785 nm excitation laser. The frequency range displayed is that corresponding to the vibrational stretching modes of the conjugated polymer backbone. All of the spectra are background-corrected and

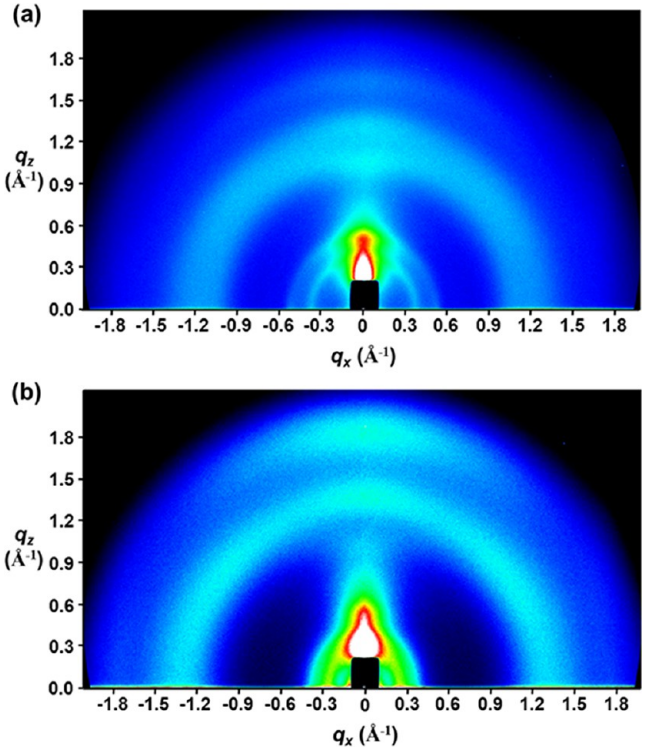

Figure 3. 2D-GIXS images of (a) PBDT-DTBTz and (b) PTIPSBDT-DTBTz films.

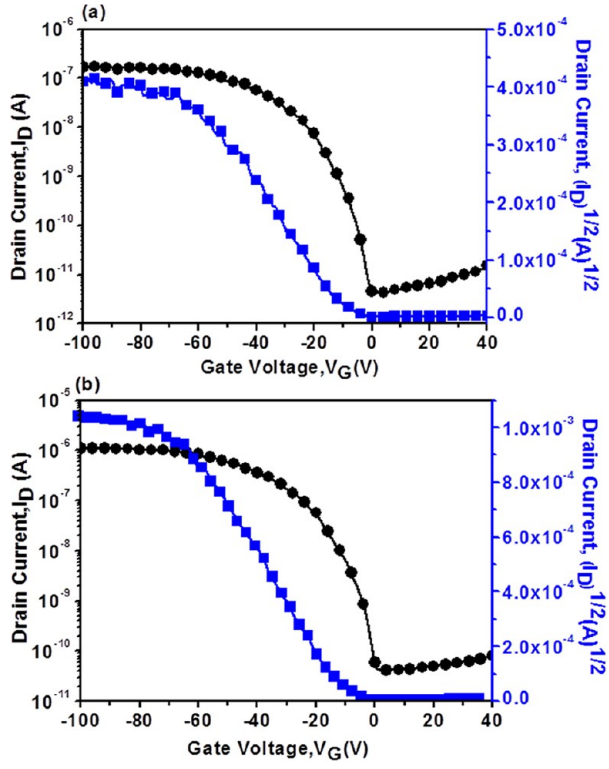

Figure 4. Transfer characteristics of OTFTs fabricated using the copolymers as the active layer at a constant source/drain voltage of −80 V: (a) PBDT-DTBTz; (b) PTIPSBDT-DTBTz.

normalized to the 1410 cm^{-1} peak, which exhibits minimal variation in the peak shape and position. The vibrational modes responsible for the observed peaks were identified using

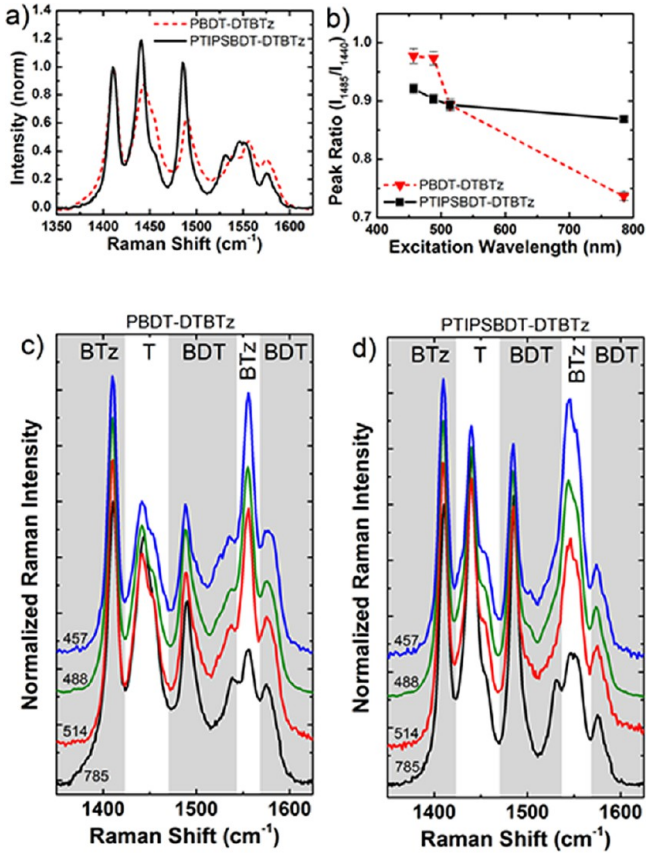

Figure 5. (a) Normalized nonresonant Raman spectra of polymer thin films measured at 785 nm excitation. (b) Ratio of peak intensities for the fused-thiophene C═C mode (1485 cm^{-1}) over the bridging thiophene C═C mode (1440 cm^{-1}) as a function of the excitation wavelength. Normalized Raman spectra of thin films for (c) PBDT-DTBTz and (d) PTIPSBDT-DTBTz measured at a range of excitation wavelengths.

frequency analysis of geometrically optimized polymer backbone segments using the *Gaussian09* software.[41] Calculations were made at the B3LYP level using the 6-311G* basis set.[42−44] The 1424−1470 cm^{-1} band of the peaks was assigned to C═C stretches in the thiophene (T) unit; the 1410 cm^{-1} peak was assigned to a vibration on the BTz unit with a strong component on the triazole part; the 1485 cm^{-1} mode was identified as a C═C symmetric stretching mode of the fused thiophene ring in the BDT unit; the mode at 1555 cm^{-1} is identified as a ring stretch of the BTz unit, while the smaller modes on either side (centered around 1535 and 1575 cm^{-1}) are ring stretches of the BDT unit associated strongly with the bonds adjacent to the site where the TIPS unit was attached. These assignments are also indicated in Figure 5c,d. PTIPSBDT-DTBTz shows an additional peak at 1545 cm^{-1}, which belongs to a delocalized backbone vibrational mode with strong components on both the BTz and BDT rings. Further discussion of these modes is provided in the Supporting Information.

The differences between the spectra in Figure 5a are attributed to the addition of the TIPS unit because this is the main difference between the two polymers. This comparison shows that adding the TIPS unit resulted in a shift of the BDT ring stretching mode at 1537 cm^{-1} by 6 cm^{-1} to lower energy. This can be understood as a reduction in the force constant of the bonds in the BDT ring caused by the addition of a bulky,

electron-withdrawing group. Adding the TIPS units also results in a measured increase in the relative intensities of the peaks at 1440 and 1485 cm^{-1} as well as a small shift to lower energies. These peaks are localized on the thiophene and fused-thiophene units, while the spectra are normalized to the 1410 cm^{-1} BTz peak. The increased relative intensity of the 1440 and 1485 cm^{-1} modes and the shifts to lower energies are indicative of increased delocalization of the π electrons on the C=C bonds between the thiophene and fused-thiophene units, suggesting a reduction in the interunit bond dihedral angle between these units.[45] In summary, the addition of the bulky TIPS units causes a lengthening of the neighboring bonds in the BDT unit and results in a reduced dihedral torsion between the T and BDT units. These interpretations are supported by DFT geometry optimization results (see the Supporting Information).

Further insight into the polymer film morphology can be gained by considering the changes in Raman spectra under different excitation conditions. In this study, four wavelengths were used (785, 514, 488, and 457 nm). Comparing these wavelengths with the absorption spectra of the thin films shown Figure 1b revealed that 785 nm lies below the absorption onset and so excites the polymer nonresonantly, whereas the shorter wavelengths fall within the absorption bands of both polymers and so selectively excite particular parts of the polymer corresponding to electronic transitions.[46] Parts c and d of Figure 5 show how the Raman spectra of PBDT-DTBTz and PTIPSBDT-DTBTz vary for different excitation wavelengths. The most pronounced effect is enhancement of the BTz ring stretching mode at 1555 cm^{-1} in PBDT-DTBTz including the 1545 cm^{-1} mode in PTIPSBDT-DTBTz. There is also a decrease in the relative intensity of the modes at 1440 and 1485 cm^{-1}. Because the spectra are normalized to the 1410 cm^{-1} BTz mode, we can say that the 1410 cm^{-1} mode shows a moderate resonant enhancement relative to the 1440 and 1485 cm^{-1} modes, while the 1555 and 1545 cm^{-1} modes show a strong resonant enhancement over all of the other modes. The resonant enhancement is associated with the electronic structure of the excited state in which the π electrons are located, and so enhancement of the BTz Raman modes (1410, 1545, and 1555 cm^{-1}) indicates that the electronic transitions corresponding to these excitation wavelengths are localized on the BTz unit and, in particular, on the main conjugated backbone benzene ring. This correlates well with localization of the calculated HOMO/LUMO transition shown in Figure 2c.

The 1485 and 1440 cm^{-1} modes also show different resonant enhancements relative to one another. This is seen most clearly in Figure 5b, showing the ratio of the peak intensities for these modes at different excitation wavelengths. For PBDT-DTBTz, we observe a strong resonant enhancement of the 1485 cm^{-1} fused-thiophene (BDT) mode relative to the 1440 cm^{-1} thiophene (T) mode. In PTIPSBDT-DTBTz, however, these modes have similar intensities for all excitation wavelengths and so there is minimal resonant enhancement. This suggests that the excited-state molecular orbital in PTIPSBDT-DTBTz is more delocalized between the BDT and T units, which is consistent with an increased planarity of the BDT-T interunit dihedral.

On the basis of these observations, it is considered that the addition of the TIPS side group results in a more planar backbone conformation of the polymer and so encourages ordered packing between neighboring molecular chains. This interpretation is consistent with the 2D-GIXS results and device characteristics, which indicate that adding the TIPS unit encouraged more ordered molecular packing.

Photovoltaic Properties. OPV cells were fabricated from PBDT-DTBTz or PTIPSBDT-DTBTz as the electron donor and $PC_{71}BM$ as the electron acceptor, with a device structure of ITO/PEDOT:PSS/polymer:$PC_{71}BM$/Ca/Al. The performance of the prepared OPVs was strongly affected by the processing parameters, including the choice of solvent, blend ratio of the polymer and $PC_{71}BM$, and processing additive effect. The performances of the OPV materials were investigated under a variety of conditions. The active layers were spin-coated from a chlorobenzene solution of the donor polymers and acceptor, with 1,8-diiodooctane (DIO) used as a processing additive for optimizing the morphology of the active layer. The fabricated devices showed the best performances at a donor-to-acceptor composition ratio of 1:1, as summarized in Table 3, with those of devices produced using alternative fabrication conditions, including different ratios, additives, solvents, and annealing conditions, summarized in Tables S1–S6 in the Supporting Information.

Table 3. Comparison of the Photovoltaic Properties of the OPVs Based on Polymer:$PC_{71}BM$ without or with a DIO Additive under Illumination of AM 1.5 G, 100 mW cm^{-2}

polymer	ratio [w/w]	DIO [3 vol %]	V_{oc}[a] [V]	J_{sc}[a] [mA cm^{-2}]	FF[a]	PCE[a] [%]
PBDT-DTBTz	1:1	no	0.77	4.93	0.43	1.63
	1:1	yes	0.77	7.87	0.48	2.88
PTIPSBDT-DTBTz	1:1	no	0.85	5.50	0.44	2.04
	1:1	yes	0.80	12.69	0.55	5.53

[a]Photovoltaic properties of polymer:$PC_{71}BM$-based devices spin-coated from a chlorobenzene solution with a device configuration of ITO/PEDOT:PSS/polymer:$PC_{71}BM$ (1:1)/Ca/Al.

Parts a and b of Figure 6 shows the current $J-V$ curves of the OPVs based on the polymer:$PC_{71}BM$ (1:1, w/w) with and without the DIO processing additive. In the absence of the additive, the devices exhibited low PCEs of 1.63 and 2.04% for PBDT-DTBTz and PTIPSBDT-DTBTz, respectively, with V_{oc} values of 0.77 and 0.85 V, respectively, which is commensurate with the measured HOMO levels of the polymers mentioned above. The PBDT-DTBTz and PTIPSBDT-DTBTz devices exhibited their J_{sc} values as 4.93 and 5.50 mA cm^{-2}, respectively.

It has been reported that the J_{sc} and FF of OPV devices could be much improved by using additives such as 1,8-diiodooctane (DIO) or 1-chloronaphthalene by forming better BHJ morphology of the active layer.[47,48] When we used 3 vol % DIO as the processing additive, the J_{sc} and FF values of both PBDT-DTBTz:$PC_{71}BM$ (1:1) and PTIPSBDT-DTBTz:$PC_{71}BM$ (1:1) devices increased dramatically. This prominent PCE improvement was likely a result of a significant increase in the J_{sc} values, i.e., from 4.93 to 7.87 mA cm^{-2} for PBDT-DTBTz:$PC_{71}BM$ (1:1) device and from 5.50 to 12.69 mA cm^{-2} for PTIPSBDT-DTBTz:$PC_{71}BM$ (1:1). The PTIPSBDT-DTBTz:$PC_{71}BM$ (1:1) device showed the highest PCEs among the fabricated devices up to 5.53%.

Parts c and d of Figure 6 show the external quantum efficiency (EQE) curves of OPVs fabricated under the same optimized conditions as those used for the $J-V$ measurements. The EQEs of the devices with DIO can be seen to be much higher than those without DIO, with the DIO-containing devices fabricated using PTIPSBDT-DTBTz exhibiting higher

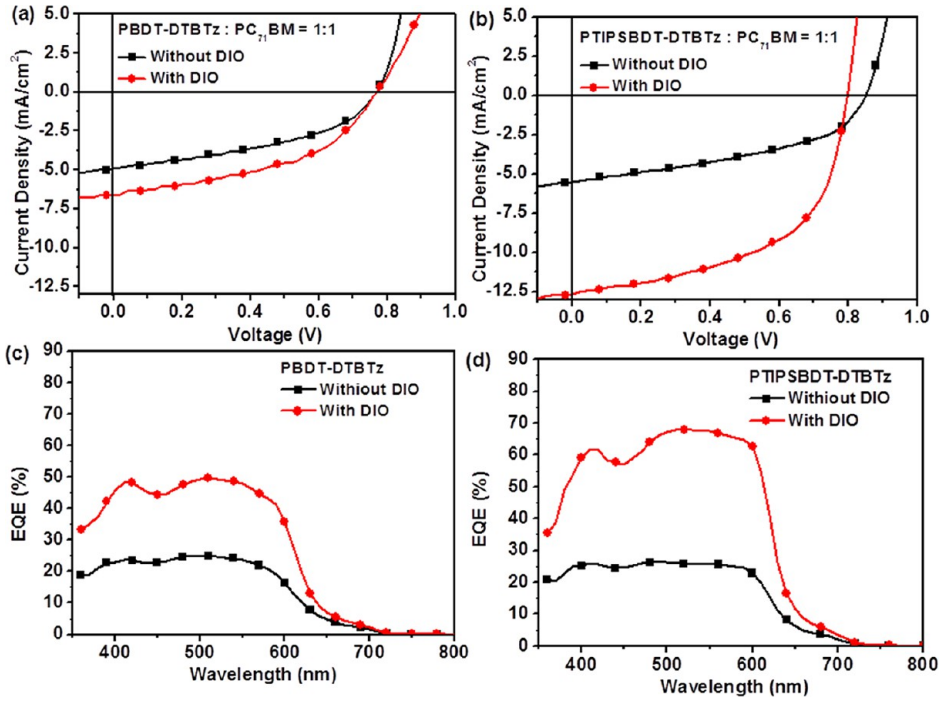

Figure 6. *J*–*V* curves of the OPVs based on (a) PBDT-DTBTz:$PC_{71}BM$ (1:1, w/w) and (b) PBDTTPS-DTBTz:$PC_{71}BM$ (1:1, w/w) with and without DIO, measured under the illumination of AM 1.5 G, 100 mW cm^{-2}. EQE curves of the OPVs based on (c) PBDT-DTBTz:$PC_{71}BM$ (1:1, w/w) and (d) PTIPSBDT-DTBTz:$PC_{71}BM$ (1:1, w/w) with and without DIO.

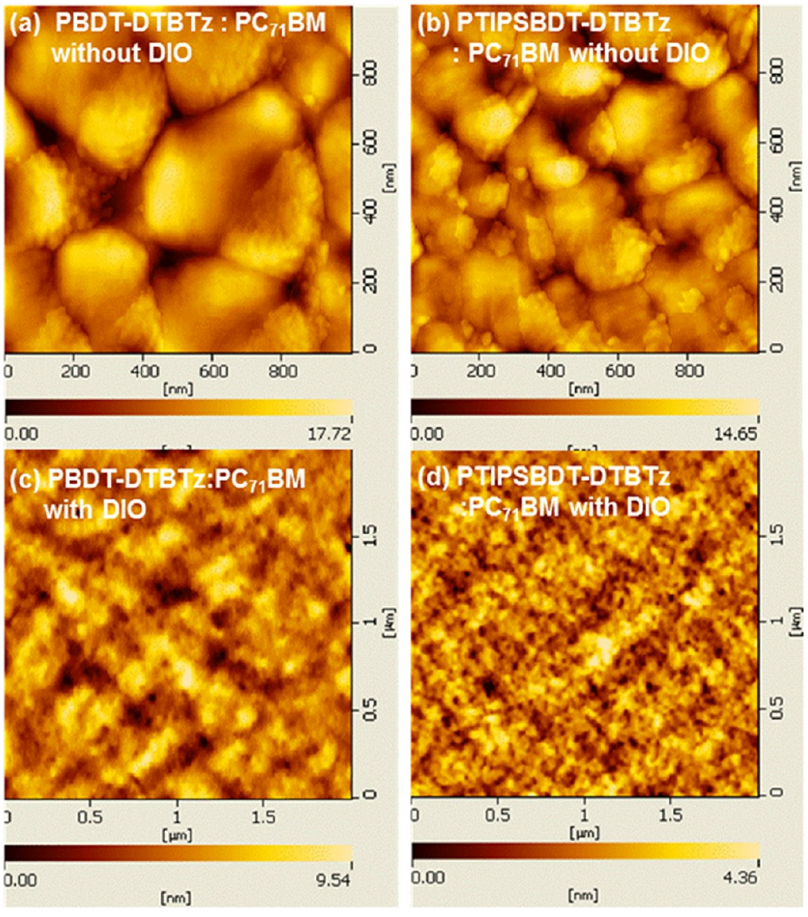

Figure 7. AFM tapping-mode height images of the blend films of (a) PBDT-DTBTz:$PC_{71}BM$ (1:1) without DIO, (b) PTIPSBDT-DTBTz:$PC_{71}BM$ (1:1) without DIO, (c) PBDT-DTBTz:$PC_{71}BM$ (1:1) with DIO, and (d) PTIPSBDT-DTBTz:$PC_{71}BM$ (1:1) with DIO.

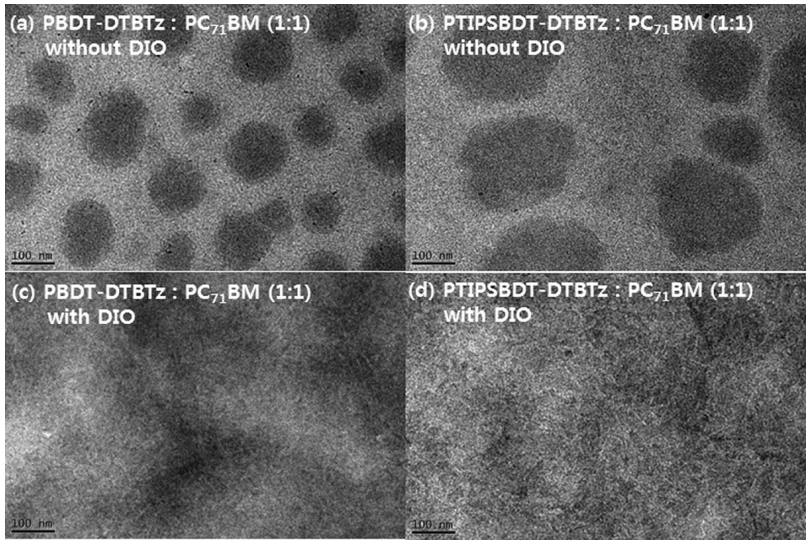

Figure 8. TEM images of polymer:$PC_{71}BM$ blends (1:1 w/w) cast from chlorobenzene: (a) PBDT-DTBTz:$PC_{71}BM$ (1:1) without DIO; (b) PTIPSBDT-DTBTz:$PC_{71}BM$ (1:1) without DIO; (c) PBDT-DTBTz:$PC_{71}BM$ (1:1) with DIO; (d) PTIPSBDT-DTBTz:$PC_{71}BM$ (1:1) with DIO.

EQEs than those using PBDT-DTBTz. In addition, the spectral responses of the OPV devices showed that photons within the range 350−700 nm contributed significantly to the EQE, with a maximum EQE of 50% (at 412 and 511 nm) and 70% (at 411 and 527 nm) for the PBDT-DTBTz and PTIPSBDT-DTBTz devices, respectively.

The morphologies of the polymer:$PC_{71}BM$ active layers were also investigated using atomic force microscopy (AFM) and transmission electron microscopy (TEM). For the films produced without DIO, the AFM topographic images reveal severe phase segregation for both polymers (Figure 7a,b). The dark regions in the TEM images of Figure 8a,b correspond to large $PC_{71}BM$ domains, which are far bigger than typical exciton diffusion lengths (∼10 nm). This would result in poor exciton dissociation and low current density. In contrast, significantly more homogeneous morphologies were found for PBDT-DTBTz:$PC_{71}BM$ and PTIPSBDT-DTBTz:$PC_{71}BM$ films processed with DIO, as shown in Figures 7c,d and 8c,d. The observed nanoscale phase separation and bicontinuous interpenetrating networks would result in more efficient charge separation and transport, leading to the much higher J_{sc} values observed. Interestingly, as can be clearly seen in Figures 7d and 8d, the formation of nanoscale networks was markedly enhanced in the PTIPSBDT-DTBTz:$PC_{71}BM$ film,[49] which explains the differences in the photovoltaic performance between the PBDT-DTBTz:$PC_{71}BM$ and PTIPSBDT-DTBTz:$PC_{71}BM$ films processed with DIO. It is evident that the DIO additive promoted optimal phase separation between the polymer and $PC_{71}BM$ and induced the formation of a fibrillar structure. It should be noted that we do not rule out other factors that could be responsible for the superior performance of the PTIPSBDT-DTBTz:$PC_{71}BM$ device because J_{sc} is known to be affected by other things such as the absorption strength of the active layer and charge-carrier mobility. The attributes of the wider absorption spectrum, stronger shoulder peak, and higher hole mobility of PTIPSBDT-DTBTz are likely to have contributed to the higher J_{sc} values compared to the PBDT-DTBTz:$PC_{71}BM$ device. Further studies are underway in order to clarify the contributions of each different factor.

CONCLUSIONS

In conclusion, we successfully synthesized two novel π-conjugated alternating copolymers via Stille coupling. The polymers were composed of unsubstituted or electron-donating TIPS-substituted BDT units and electron-accepting BTz units carrying symmetrically branched alkyl side chains. The two polymers exhibited medium band gaps (∼1.95 eV) and strong $\pi-\pi$-stacking shoulder peaks in the acquired UV−visible absorption spectra. The HOMO energy levels of the polymers were found to be relatively low compared to those of P3HT. The results demonstrate that the photovoltaic devices prepared using the polymers, in combination with fullerene derivatives, had good oxidative stability and high V_{oc} values. Upon blending with $PC_{71}BM$ and using DIO as a solvent additive, devices fabricated from PBDT-DTBTz and PTIPSBDT-DTBTz afforded PCEs of 2.88 and 5.53%, respectively. We believe that PTIPSBDT-DTBTz has a band gap similar to that of P3HT but shows significantly improved V_{oc} and PCE; thus, it is a good candidate as a medium-band-gap material for tandem OPV cells.

EXPERIMENTAL SECTION

Materials. All organic starting materials were purchased from Aldrich, Alfa Aesar, or TCI Korea and were used without further purification. The palladium catalysts were purchased from Strem, and the phenyl C_{71}-butyric acid methyl ester ($PC_{71}BM$) was purchased from EM-index. Solvents were dried and purified by fractional distillation over sodium/benzophenone and handled in a moisture-free atmosphere. Column chromatography was performed using silica gel (Merck, Kieselgel 60 63-200 MYM SC). 4,7-Dibromo-2*H*-benzo[1,2,3]triazole was synthesized according to methods described in previous reports.[22] 4,8-Dihydrobenzo[1,2-*b*:4,5-*b*′]dithiophen-4,8-dione, benzo[1,2-*b*:4,5-*b*′]dithiophene, and 4,7-dibromo-2-(heptadecan-9-yl)-2*H*-benzo[*d*][1,2,3]triazole were prepared using previously described methods.[22]

Measurements. ^{1}H and ^{13}C NMR spectra were recorded using a Varian Mercury Plus 300 MHz spectrometer, and the chemical shifts were recorded in units of ppm with chloroform as the internal standard. Elemental analysis was carried out using a Vario Micro Cube in the Korea Basic Science Institute (Busan, Korea). Mass spectra were obtained from the Agilent GC/MSD 5975C mass spectrometer. The absorption spectra were measured using a JASCO JP/V-570 model.

The molecular weights of the polymers were determined by GPC analysis relative to a polystyrene standard using a Waters high-pressure GPC assembly (model M590). TGA was carried out on a Mettler-Toledo TGA/SDTA 851^e under a dinitrogen atmosphere with a heating and cooling rate of 10 °C/min. CV was performed on a CH Instruments electrochemical analyzer. The CV measurements were carried out in acetonitrile solutions containing 0.1 M tetrabutylammonium tetrafluoroborate ($TBABF_4$) as the supporting electrolyte, Ag/$AgNO_3$ as the reference electrode, a platinum wire as the counter electrode, and platinum as the working electrode. The polymer films were coated on the platinum working electrode.

2D-GIXS Experiments. 2D-GIXS measurements were performed on Beamline 4C-2 at the Pohang Accelerator Laboratory (South Korea). X-rays with a wavelength of 1.1179 Å (11.09 keV) were used. The incidence angle (0.28°) was chosen to allow for complete penetration of the X-rays into the polymer film. A thin layer (40−50 nm) of PEDOT:PSS was spin-coated onto silicon substrates, with the polymer thin films subsequently spin-coated on top.

Fabrication of Field-Effect Transistor Devices. The hole mobilities of the synthesized polymers were measured by fabricating OTFTs using the same fabrication conditions as those described in the previous report.[24]

Resonant Raman Spectroscopy. Thin-film samples were prepared by spin-coating from 10 mg/mL chloroform solutions onto Spectrosil 2000 substrates to a thickness of 50 nm. Raman spectra were measured with a Renishaw inVia Raman microscope using a 50× objective. Excitation conditions were as follows: 785 nm, 100 mW, exposure time 60 s; 514 nm, 0.7 mW, exposure time 60 s; 488 nm, 90 μW, exposure time 40 s; 457 nm, 110 μW, exposure time 50 s. For 488 and 457 nm excitation, the laser beam was defocused to a diameter of ∼10 μm to minimize photodegradation. The spectral resolution is 1 cm^{-1}.

Fabrication of Photovoltaic Devices. The devices were fabricated with the structure ITO/PEDOT:PSS/polymer:$PC_{71}BM$/Ca/Al. The procedure for cleaning the ITO surface included sonication and rinsing in distilled H_2O, methanol, and acetone. The hole-transporting PEDOT:PSS layer (45 nm) was spin-coated onto each ITO anode from a solution purchased from Heraeus (Clevios P). Each polymer:$PC_{71}BM$ solution was then spin-coated onto the PEDOT:PSS layer. The polymer solution for spin coating was prepared by dissolving the polymer (8 mg/mL) in chlorobenzene/DIO (97:3). Calcium and aluminum contacts were formed sequentially by vacuum deposition at a pressure of $<3 \times 10^{-6}$ Torr, providing an active area of 0.09 cm^2. The thickness of the active layer was measured by using a KLA Tencor Alpha-step IQ surface profilometer with an accuracy of ±1 nm. The current density−voltage (J−V) characteristics of all of the polymer photovoltaic cells were determined by illuminating the cells with simulated solar light (AM 1.5 G) with an intensity of 100 mW/cm^2 using an Oriel 1000 W solar simulator. Electronic data were recorded using a Keithley 236 source-measure unit, and all characterizations were carried out in an ambient environment. The illumination intensity was calibrated by employing a standard silicon photodiode detector from PV measurements Inc., which was calibrated at the National Renewable Energy Laboratory. The EQE was measured as a function of the wavelength in the range 360−800 nm using a halogen lamp as the light source, and the calibration was performed by using a silicon reference photodiode. All of the characterization steps were carried out in an ambient laboratory atmosphere.

Synthesis of Monomers and Polymers. *Synthesis of 2-(Heptadecan-9-yl)-4,7-bis(thiophen-2-yl)-2H-benzo[d][1,2,3]triazole (**1**).* *N*-Tripropyl(thiophen-2-yl)stannane (1.60 g, 4.85 mmol) was added to a stirred solution of 4,7-dibromo-2,1,3-benzothiadiazole (1.00 g, 1.90 mmol) and bis(triphenylphosphine)palladium(II) dichloride (95 mg, 0.06 mmol) in toluene (50 mL). The mixture was refluxed overnight and then extracted with ethyl acetate. The organic layer was washed with $NaHCO_3$ and brine and then dried over anhydrous $MgSO_4$. The solvent was removed, and the crude product was purified using column chromatography on silica with hexane as the eluent, to yield **2** (1.5 g, 58%) as a pale-yellow solid.

^{1}H NMR (300 MHz, $CDCl_3$): δ 8.05 (d, 2H), 7.65 (s, 2H), 7.31 (d, 2H), 7.23 (t, 2H), 4.90 (m, 1H), 2.35 (m, 2H), 2.01 (m, 2H), 1.31−1.21 (m, 22H), 1.08−0.96 (m, 2H), 0.86 (t, 6H). ^{13}C NMR (75 MHz, $CDCl_3$): δ 147.8, 140.2, 132.8, 130.5, 129.2, 125.0, 69.54, 35.59, 31.75, 29.22, 29.14, 29.01, 26.05, 22.62, 14.16. Anal. Calcd for $C_{31}H_{43}N_3S_2$: C, 71.35; H, 8.31; N, 8.05; S, 12.29. Found: C, 70.88; H, 8.25; N, 7.98; S, 12.11.

Synthesis of 4,7-Bis(5-bromothiophen-2-yl)-2-(heptadecan-9-yl)-2H-benzo[d][1,2,3]triazole (DTBTz). *N*-Bromosuccinimide (1.02 g, 4.79 mmol) was added to a stirred solution of compound **2** (1.00 g, 1.92 mmol) in *N*,*N*-dimethylformamide (DMF; 25 mL) in the absence of light. The mixture was stirred at room temperature for 4 h, and a bright-yellow solid precipitate was formed. The mixture was filtered and washed thoroughly with methanol. The solid was then washed once with cold diethyl ether and purified by flash chromatography to give DTBTz (1.80 g, 80%). ^{1}H NMR (300 MHz, $CDCl_3$): δ 7.81 (d, 2H), 7.50 (s, 2H), 7.11 (d, 2H), 4.90 (m, 1H), 2.35 (m, 2H), 2.01 (m, 2H), 1.31−1.21 (m, 22H), 1.08−0.96 (m, 2H), 0.86 (t, 6H). ^{13}C NMR (75 MHz, $CDCl_3$): δ 147.5, 144.2, 140.5, 135.5, 133.1, 128.0, 115.6, 70.32, 38.61, 35.15, 30.28, 30.10, 29.52, 27.11, 26.32, 12.18. Anal. Calcd for $C_{31}H_{41}Br_2N_3S_2$: C, 54.79; H, 6.08; N, 6.18; S, 9.44. Found: C, 55.01; H, 6.00; N, 5.99; S, 8.74. MS (GC, $C_{31}H_{41}Br_2N_3S_2$): calcd, 679.6; found, 679.3.

Synthesis of 2,6-Bis(trimethylstannyl)benzo[1,2-b:4,5-b′]-dithiophene (BDT). A total of 1.00 g (2.6 mmol) of benzo[1,2-*b*;4,5-*b*′]dithiophene was dissolved in anhydrous tetrahydrofuran (THF; 20 mL) under an argon atmosphere. The mixture was cooled to −78 °C, and then a 1.6 M solution of *n*-butyllithium (8.2 mL, 6.6 mmol) in hexane was added, forming a white precipitate. After 2 h at −78 °C, trimethyltin chloride (3.10 g, 7.80 mmol) was added. The solution was left in a cold bath to warm to room temperature overnight. Diethyl ether (50 mL) was then added to the solution, and it was extracted with brine and H_2O. The organic solvent was evaporated, and the residue was recrystallized from acetonitrile three times, yielding the product (1.58 g, 59%) as colorless platelets. ^{1}H NMR (300 MHz, CD_2Cl_2): δ 8.30 (s, 2H), 7.46 (s, 2H), 0.46 (s, 18H). ^{13}C NMR (75 MHz, CD_2Cl_2): δ 142.7, 141.9, 139.2, 131.5, 115.5, −8.1. Anal. Calcd for $C_{16}H_{22}S_2Sn_2$: C, 37.25; H, 4.30; S, 12.43; Sn, 46.02. Found: C, 37.20; H, 4.21; S, 12.39. MS (GC, $C_{16}H_{22}S_2Sn_2$): calcd, 515.9; found, 516.0.

*Synthesis of 4,8-Bis[(triisopropylsilyl)ethynyl]benzo[1,2-b:4,5-b′]-dithiophene (**2**).* An oven-dried 500 mL round-bottomed flask equipped with a stirbar was cooled to 0 °C. Under an argon atmosphere, THF (50 mL) and (triisopropylsilyl)acetylene (6.7 mL, 29.9 mmol) were added, followed by the dropwise addition of a 1.6 M solution of *n*-buyllithium (19.3 mL, 32.7 mmol) in hexane. This mixture was stirred for 2 h, and then THF (120 mL) and benzo[1,2-*b*:4,5-*b*′]dithiophene-4,8-dione (5 g, 13.7 mmol) were added. The mixture was stirred at room temperature for 24 h and then quenched with H_2O. The resulting mixture was poured into a saturated NH_4Cl solution and extracted with ethyl acetate. The organic layer was washed with brine and dried over anhydrous $MgSO_4$. The solvent was evaporated, the residue was dissolved in THF (120 mL), and then $SnCl_2{\cdot}2H_2O$ (15.3 g, 68.1 mmol, in 50 mL 50% acetic acid) was added dropwise. The mixture was stirred at room temperature overnight, then poured into H_2O, and extracted with ethyl acetate. The organic layer was washed with $NaHCO_3$ and brine and then dried over anhydrous $MgSO_4$. The organic solvent was removed, and the crude product was purified using column chromatography on silica with hexane as the eluent, to yield **2** (3.6 g, 48%) as a pale-green solid. ^{1}H NMR (300 MHz, $CDCl_3$): δ 7.61 (d, 2H), 7.56 (d, 2H), 1.23 (m, 42H). ^{13}C NMR (75 MHz, $CDCl_3$): δ 140.86, 138.51, 128.28, 123.14, 112.18, 102.63, 101.62, 18.78, 11.33. Anal. Calcd for $C_{36}H_{46}S_2Si_2$: C, 69.75; H, 8.41; S, 11.64. Found: C, 69.71; H, 8.40; S, 11.63.

Synthesis of 2,6-Bis(trimethyltin)-4,8-bis[(triisopropylsilyl)-ethynyl]benzo[1,2-b:4,5-b′]dithiophene (TIPSBDT). Under an argon atmosphere, a 1.6 M solution of *n*-butyllithium (5.1 mL, 8.1 mmol) in hexane was added dropwise via syringe to compound **3** (1.5 g, 2.7 mmol) and tetramethylethylenediamine (1.2 mL, 8.1 mmol) in THF (30 mL), which was cooled to −78 °C. After stirring at this

temperature for 30 min, a 1 M solution of trimethyltin chloride (10.8 mL, 10.8 mmol) in THF was added in one portion After being allowed to warm to room temperature overnight, the reaction mixture was poured into H_2O (50 mL), and then ethyl acetate (50 mL) was added. The organic layer was washed twice with H_2O (50 mL) and dried with anhydrous $MgSO_4$. The organic layer was evaporated, and the product was then dried in a vacuum oven to afford the product (1.9 g, 80%) as a pale-yellow solid. ^{1}H NMR (300 MHz, $CDCl_3$): δ 7.69 (s, 2H), 1.23 (m, 42H), 0.47 (s, 18H). ^{13}C NMR (75 MHz, $CDCl_3$): δ 144.68, 143.51, 139.10, 110.36, 103.33, 100.64, 19.06, 11.39, −8.3. Anal. Calcd for $C_{38}H_{62}S_2Si_2Sn_2$: C, 52.06; H, 7.13; S, 7.32. Found: C, 52.09; H, 7.11; S, 7.29. MS (GC, $C_{38}H_{62}S_2Si_2Sn_2$): calcd, 876.6; found, 876.4.

General Polymerization Procedure. All polymers were synthesized by Stille polymerization, as shown in Scheme 3. The BDT, TIPSBDT, and DTBTz monomers were synthesized according to previous reports.[24] A mixture of tetrakis(triphenylphosphine)palladium in a mixed solvent of anhydrous toluene (12 mL) and anhydrous DMF (3 mL) was stirred at 120 °C under dinitrogen for 2 days, then excess 2-bromothiophene and triisopropyl(thiophen-2-yl)stannane were added and dissolved in anhydrous toluene (1 mL), and the reaction was continued for 12 h. After completion of polymerization, the reaction mixture was cooled to approximately 50 °C and methanol (200 mL) was added slowly with vigorous stirring. The precipitated polymers were collected by filtration, dissolved in chloroform, and reprecipitated in methanol and then acetone. The polymers were further purified by washing for 2 days in a Soxhlet apparatus, with acetone used to remove oligomers and catalyst residues. The reprecipitation in chloroform/methanol was then repeated several times. The resulting polymers were found to be soluble in common organic solvents.

Poly{benzo[1,2-b:4,5-b′]dithiophene-alt-2-(heptadecan-9-yl)-4,7-bis(thiophen-2-yl)-2H-benzo[d][1,2,3]triazole} (PBDT-DTBTz). 2,6-Bis(trimethylstannyl)benzo[1,2-*b*:4.5-*b*′]dithiophene (400 mg, 0.78 mmol) was mixed with DTBTz (526 mg, 1.0 equiv), tetrakis-(triphenylphosphine)palladium (3.0 mg, 2.6 μmol), toluene (12 mL), and DMF (3 mL) for polymerization. ^{1}H NMR (300 MHz, CD_2Cl_2): δ 8.30−7.59 (br, 4H), 7.48−7.25 (br, 4H), 7.23−7.21 (br, 2H), 4.98 (br, 1H), 2.42−1.90 (br, 4H), 1.40−0.90 (br, 24H), 0.84−0.81 (br, 6H). Anal. Calcd: C, 69.35; H, 6.67; N, 5.92; S, 18.06. Found: C, 69.89; H, 6.95; N, 5.30; S, 18.60.

Poly{4,8-Bis[(triisopropylsilyl)ethynyl)benzo[1,2-b:4,5-b′]-dithiophene-alt-2-(heptadecan-9-yl)-4,7-bis(thiophen-2-yl)-2H-benzo[d][1,2,3]triazole} (PTIPSBDT-DTBTz). TIPSBDT (400 mg, 0.78 mmol) was mixed with DTBTz (310 mg, 1.0 equiv), tetrakis-(triphenylphosphine)palladium (3.0 mg, 2.6 μmol), toluene (12 mL), and DMF (3 mL) for polymerization. ^{1}H NMR (300 MHz, CD_2Cl_2): δ 7.90−7.66 (br, 4H), 7.50−7.21 (br, 2H), 7.19−7.11 (br, 2H), 4.95 (br, 1H), 2.45−1.95 (br, 4H), 1.42−0.89 (br, 66H), 0.83−0.80 (br, 6H). Anal. Calcd: C, 70.66; H, 8.19; N, 3.92; S, 11.98. Found: C, 71.20; H, 8.42; N, 4.28; S, 10.69.

■ ASSOCIATED CONTENT

Ⓢ Supporting Information

MS spectra, TGA, CV curves, and OPV parameter data. This material is available free of charge via the Internet at http://pubs.acs.org.

■ AUTHOR INFORMATION

Corresponding Author

*Tel.: +82 51 510 2232. Fax: +82 51 516 7421. E-mail: dohoonhwang@pusan.ac.kr.

Notes

The authors declare no competing financial interest.

■ ACKNOWLEDGMENTS

This work was supported by a grant (Grant 2012055225) from the Center for Advanced Soft Electronics under the Global Frontier Research Program of the Ministry of Education, Science and Technology, Korea, and a grant from New and Renewable Energy Program of the Korea Institute of Energy Technology Evaluation and Planning funded by the Ministry of Knowledge Economy (Grant 20113010010030) and also supported by the World Class University program in Korea (Grant R32-10051).

■ REFERENCES

(1) Li, J.; Zhao, Y.; Tan, H. S.; Guo, Y.; Di, C.-A.; Yu, G.; Liu, Y.; Lin, M.; Lim, S. H.; Zhou, Y.; Su, H.; Ong, B. S. *Sci. Rep.* **2012**, *2*, 754.
(2) Chen, H.; Guo, Y.; Yu, G.; Zhao, Y.; Zhang, J.; Gao, D.; Liu, H.; Liu, Y. *Adv. Mater.* **2012**, *24*, 4618−4622.
(3) He, Z.; Zhong, C.; Su, S.; Xu, M.; Wu, H.; Cao, Y. *Nat. Photonics* **2012**, *6*, 591−595.
(4) Li, G.; Zhu, R.; Yang, Y. *Nat. Photonics* **2012**, *6*, 153−161.
(5) Guenes, S.; Neugebauer, H.; Sariciftci, N. S. *Chem. Rev.* **2007**, *107*, 1324−1338.
(6) Chen, H. Y.; Hou, J. H.; Zhang, S. Q.; Liang, Y. Y.; Yang, G. W.; Yang, Y.; Yu, L. P.; Wu, Y.; Li, G. *Nat. Photonics* **2009**, *3*, 649−653.
(7) Liang, Y. Y.; Xu, Z.; Xia, J. B.; Tsai, S. T.; Wu, Y.; Li, G.; Ray, C.; Yu, L. P. *Adv. Mater.* **2010**, *22*, E135−E138.
(8) You, J. B.; Li, X. H.; Xie, F. X.; Sha, W. E. I.; Kwong, J. H. W.; Li, G.; Choy, W. C. H.; Yang, Y. *Adv. Energy Mater.* **2012**, *2*, 1203−1207.
(9) Li, X. H.; Choy, W. C. H.; Huo, L. J.; Xie, F. X.; Sha, W. E. I.; Ding, B. F.; Guo, X.; Li, Y.; Hou, J. H.; You, J. B.; Yang, Y. *Adv. Mater.* **2012**, *24*, 3046−3052.
(10) He, Z. C.; Zhong, C. M.; Su, S. J.; Xu, M.; Wu, H. B.; Cao, Y. *Nat. Photonics* **2012**, *6*, 591−596.
(11) Li, Y. *Acc. Chem. Res.* **2012**, *45*, 723−733.
(12) Scharber, M. C.; Mühlbacher, D.; Koppe, M.; Denk, P.; Waldauf, C.; Heeger, A. J.; Brabec, C. J. *Adv. Mater.* **2006**, *18*, 789−794.
(13) Wong, W.-Y.; Ho, C.-L. *Acc. Chem. Res.* **2010**, *43*, 1246−1256.
(14) Cui, C.; Min, J.; Ho, C.-L.; Ameri, T.; Yang, P.; Zhao, J.; Brabec, C. J.; Wong, W.-Y. *Chem. Commun.* **2013**, *49*, 4409−4411.
(15) Ye, D.; Li, X.; Yan, L.; Zhang, W.; Hu, Z.; Liang, Y.; Fang, J.; Wong, W.-Y.; Wang, X. *J. Mater. Chem. A* **2013**, *1*, 7622−7629.
(16) Blouin, N.; Michaud, A.; Gendron, D.; Wakim, S.; Blair, E.; Neagu-Plesu, R.; Belletete, M.; Durocher, G.; Tao, Y.; Leclerc, M. *J. Am. Chem. Soc.* **2008**, *130*, 732−742.
(17) Moon, J. S.; Jo, J.; Heeger, A. J. *Adv. Energy Mater.* **2012**, *2*, 304−308.
(18) Price, S. C.; Stuart, A. C.; Yang, L.; Zhou, H.; You, W. *J. Am. Chem. Soc.* **2011**, *133*, 4625−4631.
(19) He, Y.; Chen, H. Y.; Hou, J.; Li, Y. *J. Am. Chem. Soc.* **2010**, *132*, 1377−1382.
(20) Zhao, X.; Yang, D.; Lv, H.; Yin, L.; Yang, X. *Polym. Chem* **2013**, *4*, 57−60.
(21) Min, J.; Zhang, Z.-G.; Zhang, S.; Zhang, M.; Zhang, J.; Li, Y. *Macromolecules* **2011**, *44*, 7632−7638.
(22) Kim, J.-H.; Kim, H. U.; Song, C. U.; Shin, W. S.; Lee, J.-K.; Kang, I.-N.; Lee, J.-K.; Hwang, D.-H. *Sol. Energy Mater. Sol. Cells* **2013**, *108*, 113−125.
(23) Anthony, J. E. *Chem. Rev.* **2006**, *106*, 5028−5048.
(24) Anthony, J. E. *Angew. Chem., Int. Ed.* **2008**, *47*, 452−483.
(25) Chung, D. S.; Park, J. W.; Yun, W. M.; Cha, H.; Kim, Y.-H.; Kwon, S.-K.; Park, C. E. *ChemSusChem* **2010**, *3*, 742−748.
(26) Winzenberg, K. N.; Kemppinen, P.; Fanchini, G.; Bown, M.; Collis, G. E.; Forsyth, C. M.; Hegedus, K.; Singh, T. B.; Watkins, S. E. *Chem. Mater.* **2009**, *21*, 5701−5703.
(27) Park, J.-H.; Chung, D. S.; Lee, D. H.; Kong, H.; Jung, I. H.; Park, M.-J.; Cho, N. S.; Park, C. E.; Shim, H.-K. *Chem. Commun.* **2010**, *46*, 1863−1865.
(28) Shi, Q.; Fan, H.; Liu, Y.; Hu, W.; Li, Y.; Zhan, X. *Macromolecules* **2011**, *44*, 9173−9179.
(29) Bathula, C.; Song, C. E.; Badgujar, S.; Hong, S.-J.; Kang, I.-N.; Moon, S.-J.; Lee, J.; Cho, S.; Shim, H.-K.; Lee, S. K. *J. Mater. Chem.* **2012**, *22*, 22224−22232.

(30) Delley, B. J. *J. Chem. Phys.* **1990**, *92*, 508−517.
(31) Perdew, J. P.; Wang, Y. *Phys. Rev. B* **1992**, *45*, 13244−13249.
(32) Perdew, J. P.; Burke, K.; Ernzerhof, M. *Phys. Rev. Lett.* **1996**, *77*, 3865−3868.
(33) Kim, J.-H.; Lee, S.; Kang, I.-N.; Park, M.-J.; Hwang, D.-H. *J. Polym. Sci., Part A: Polym. Chem.* **2012**, *50*, 3415−3424.
(34) Hou, J.; Tan, Z.; Yan, Y.; He, Y.; Yang, C.; Li, Y. *J. Am. Chem. Soc.* **2006**, *128*, 4911−4916.
(35) Zhou, H.; Yang, L.; You, W. *Macromolecules* **2012**, *45*, 607−632.
(36) Clarke., T. M.; Durrant, J. R. *Chem. Rev.* **2010**, *110*, 6736−6767.
(37) Cho, H.-H.; Kang, T. E.; Kim, K.-H.; Kang, H.; Kim, H. J.; Kim, B. *Macromolecules* **2012**, *45*, 6415−6417.
(38) Shaw, J. M.; Seidler, P. F. *IBM J. Res. Dev.* **2001**, *45*, 3−9.
(39) Dimitrakopoulos, C. D.; Mascaro, D. J. *IBM J. Res. Dev.* **2001**, *45*, 11−27.
(40) Coakley, K. M.; McGehee, M. D. *Chem. Mater.* **2004**, *16*, 4533−4542.
(41) Frisch, M. J.; Trucks, G. W.; Schlegel, H. B.; Scuseria, G. E.; Robb, M. A.; Cheeseman, J. R.; Scalmani, G.; Barone, V.; Mennucci, B.; Petersson, G. A.; Nakatsuji, H.; Caricato, M.; Li, X.; Hratchian, H. P.; Izmaylov, A. F.; Bloino, J.; Zheng, G.; Sonnenberg, J. L.; Hada, M.; Ehara, M.; Toyota, K.; Fukuda, R.; Hasegawa, J.; Ishida, M.; Nakajima, T.; Honda, Y.; Kitao, O.; Nakai, H.; Vreven, T.; Montgomery, J. A., Jr.; Peralta, J. E.; Ogliaro, F.; Bearpark, M.; Heyd, J. J.; Brothers, E.; Kudin, K. N.; Staroverov, V. N.; Kobayashi, R.; Normand, J.; Raghavachari, K.; Rendell, A.; Burant, J. C.; Iyengar, S. S.; Tomasi, J.; Cossi, M.; Rega, N.; Millam, J. M.; Klene, M.; Knox, J. E.; Cross, J. B.; Bakken, V.; Adamo, C.; Jaramillo, J.; Gomperts, R.; Stratmann, R. E.; Yazyev, O.; Austin, A. J.; Cammi, R.; Pomelli, C.; Ochterski, J. W.; Martin, R. L.; Morokuma, K.; Zakrzewski, V. G.; Voth, G. A.; Salvador, P.; Dannenberg, J. J.; Dapprich, S.; Daniels, A. D.; Farkas, Ö.; Foresman, J. B.; Ortiz, J. V.; Cioslowski, J.; Fox, D. J. *Gaussian09*, revision A.1; Gaussian, Inc.: Wallingford, CT, 2009.
(42) Kohn, W.; Becke, A. D.; Parr, R. G. *J. Phys. Chem.* **1996**, *100*, 12974−12980.
(43) Becke, A. *Phys. Rev. A* **1988**, *38*, 3098−3100.
(44) Lee, C.; Yang, W.; Parr, R. G. *Phys. Rev. B* **1988**, *37*, 785−789.
(45) Tsoi, W. C.; James, D. T.; Kim, J. S.; Nicholson, P. G.; Murphy, C. E.; Bradley, D. D. C.; Nelson, J.; Kim, J.-S. *J. Am. Chem. Soc.* **2011**, *133*, 9834−9843.
(46) Reish, M. E.; Nam, S.; Lee, W.; Woo, H. Y.; Gordon, K. C. *J. Phys. Chem. C* **2012**, *116*, 21255−21266.
(47) Kim, J.-H.; Song, C. E.; Kang, I.-N.; Shin, W. S.; Hwang, D.-H. *Chem. Commun.* **2013**, *49*, 3248−3250.
(48) Hou, J.; Park, M. H.; Zhang, S.; Yao, Y.; Chen, L. M.; Li, J. H.; Yang, Y. *Macromolecules* **2008**, *41*, 6012−6018.
(49) Kim, J.-H.; Song, C. E.; Kim, H. U.; Grimsdale, A. C.; Moon, S.-J.; Shin, W. S.; Choi, S. K.; Hwang, D.-H. *Chem. Mater.* **2013**, *25*, 2722−2732.